

1 **Strong light scattering of highly oxygenated organic aerosols impacts**  
2 **significantly on visibility degradation**

3 **Li Liu<sup>1</sup>, Ye Kuang<sup>2,3\*</sup>, Miaomiao Zhai<sup>2,3</sup>, Biao Xue<sup>2,3</sup>, Yao He<sup>2,3</sup>, Jun Tao<sup>2,3</sup>, Biao**  
4 **Luo<sup>2,3</sup>, Wanyun Xu<sup>4</sup>, Jiangchuan Tao<sup>2,3</sup>, Changqin Yin<sup>1,7</sup>, Fei Li<sup>1,5</sup>, Hanbing Xu<sup>6</sup>,**  
5 **Tao Deng<sup>1</sup>, Xuejiao Deng<sup>1</sup>, Haobo Tan<sup>1</sup>, Min Shao<sup>2,3</sup>**

6 <sup>1</sup> Institute of Tropical and Marine Meteorology, China Meteorological Administration,  
7 Guangzhou, 510640, China

8 <sup>2</sup> Institute for Environmental and Climate Research, Jinan University, Guangzhou,  
9 China.

10 <sup>3</sup> Guangdong-Hongkong-Macau Joint Laboratory of Collaborative Innovation for  
11 Environmental Quality, Guangzhou, China.

12 <sup>4</sup> State Key Laboratory of Severe Weather & Key Laboratory for Atmospheric  
13 Chemistry, Institute of Atmospheric Composition, Chinese Academy of Meteorological  
14 Sciences, Beijing, 100081, China

15 <sup>5</sup> Xiamen Key Laboratory of Straits Meteorology, Xiamen Meteorological Bureau,  
16 Xiamen, 361012, China

17 <sup>6</sup> Experimental Teaching Center, Sun Yat-Sen University, Guangzhou 510275, China

18 <sup>7</sup> Shanghai Key Laboratory of Meteorology and Health, Shanghai Meteorological  
19 Bureau, Shanghai 200030, China

20 \*Correspondence to: Ye Kuang (kuangye@jnu.edu.cn)

21

22

23

24

25

26

27

28

29

30

31

32

33	<b>Table of contents</b>	
34	<b>1. Site information.....</b>	<b>3</b>
35	<b>Figure S1.</b> Site environments and the container (green one).....	<b>3</b>
36	<b>2.Q-ACSM analysis .....</b>	<b>3</b>
37	<b>Figure S2.</b> Diagnostic plots of the 4-factor solution in the unconstrained PMF. ....	<b>6</b>
38	<b>PMF results.....</b>	<b>7</b>
39	<b>Figure S3.</b> Mass spectra, diurnal variations and time series of 3-factor solution from	
40	unconstrained PMF.....	<b>7</b>
41	<b>Figure S4.</b> Mass spectra, diurnal variations, and time series of 4-factor solution from	
42	unconstrained PMF.....	<b>8</b>
43	<b>Figure S5.</b> Mass spectra, diurnal variations, and time series of 5-factor solution from	
44	unconstrained PMF. ....	<b>9</b>
45	<b>Figure S6.</b> Diagnostic plots of the 5-factor solution in the unconstrained PMF during the spring	
46	festival period from 11th to 25th February 2021.....	<b>10</b>
47	<b>Figure S7.</b> Mass spectra, diurnal variations, and time series of 5-factor solution from	
48	unconstrained PMF during the spring festival period from 11 <sup>th</sup> to 25 <sup>th</sup> February 2021. ....	<b>11</b>
49	<b>ME-2 results.....</b>	<b>12</b>
50	<b>Figure S8.</b> Mass spectra, diurnal variations, and time series of ME-2(a-value=0.1) under	
51	the 4-factor solution. ....	<b>12</b>
52	<b>Figure S9.</b> Mass spectra, diurnal variations, and time series of ME-2(a-value=0.2) under	
53	the 4-factor solution. ....	<b>13</b>
54	<b>Figure S10.</b> Mass spectra, diurnal variations, and time series of ME-2(a-value=0.3) under	
55	the 4-factor solution. ....	<b>14</b>
56	<b>3. Discussions on traditional multilinear regression model .....</b>	<b>14</b>
57	<b>Table S1.</b> Square of correlation coefficients between aerosol components.....	<b>15</b>
58	<b>Table S2.</b> Square of correlation coefficients between changes of aerosol components for	
59	identified cases.....	<b>16</b>
60	<b>4. Visibility contributions estimation .....</b>	<b>16</b>
61	<b>5. Other Figures .....</b>	<b>18</b>
62	<b>Figure S11.</b> Simulated relationships between $VSE_{PM1}$ and $R_{sca}$ using Mie theory through	
63	varying volume geometric mean $D_{gv}$ of lognormal size distributions from 100 to 700 nm under	
64	different standard deviation ( $\sigma_g$ ) conditions.....	<b>19</b>
65	<b>Figure S12.</b> Histogram of ambient relative humidity (RH) during the observation period. ...	<b>20</b>
66	<b>Figure S13.</b> Aerosol light scattering enhancement measurements (fRH) at 525 nm from 13 <sup>th</sup> to	
67	26 <sup>th</sup> February with RH range of 60-90%.....	<b>21</b>
68	<b>References .....</b>	<b>22</b>
69		
70		
71		
72		

73 **1. Site information**

74 The observation site locates in Haizhu wetland park, which is surrounded by roads,  
75 business, and residential districts, however, at least ~1 km away from the observation  
76 site.



77 **Figure S1.** Site environments and the container (green one).

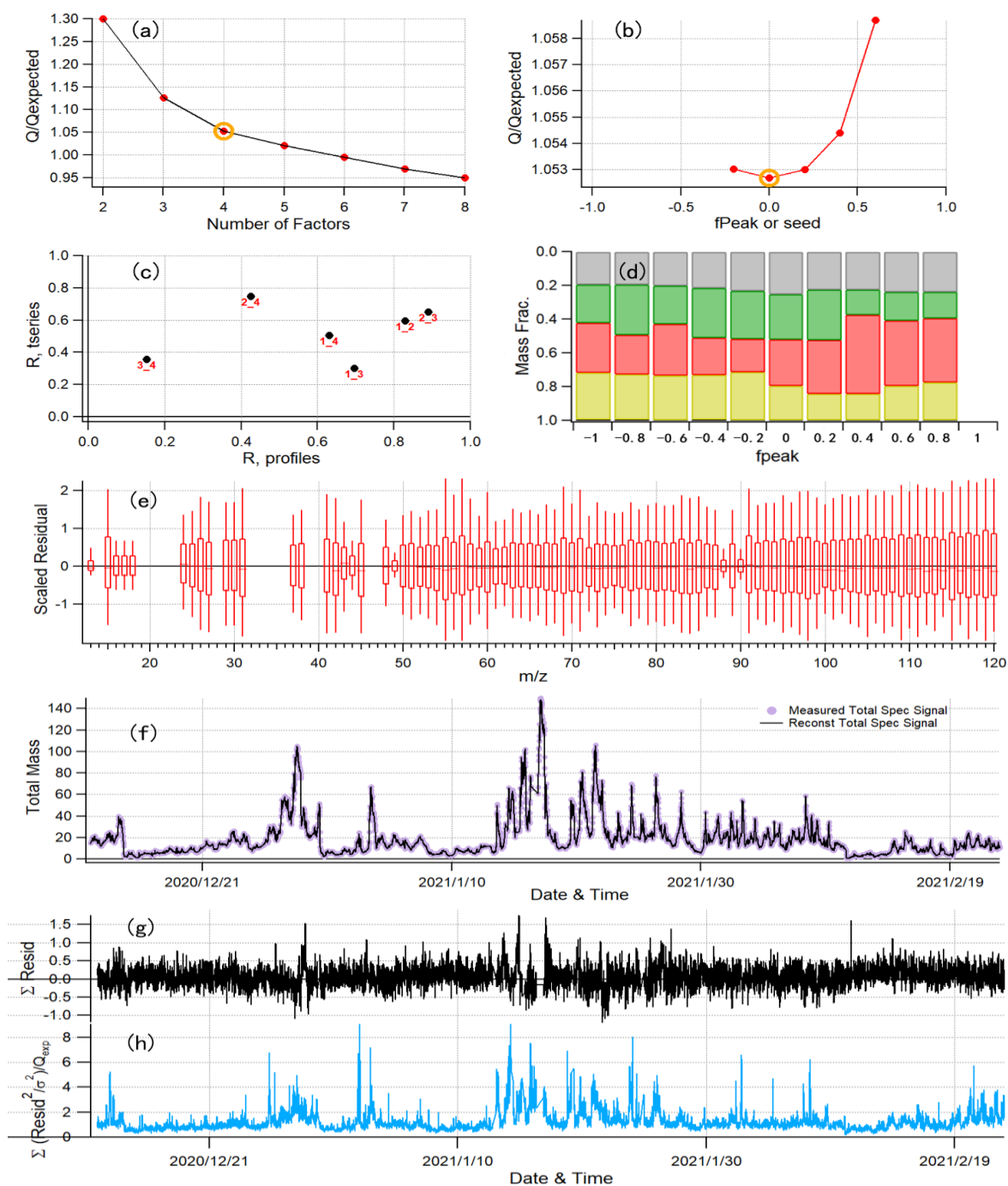
78  
79  
80

81 **2.Q-ACSM analysis**

82 In this study, organic aerosol (OA) spectra measured by the Q-ACSM were  
83 deconvolved into OA factors using an improved source apportionment technique called  
84 Multilinear Engine (ME-2) which is an upgrade of widely used Positive Matrix  
85 Factorization (PMF) technique and runs on a IGOR-based interface <sup>1</sup>. Different with  
86 traditional PMF, ME-2 offers a coefficient called a-value to constrain the spectra

87 variation extent of OA factor with given priori mass spectra<sup>1,2</sup>. The unconstrained runs  
88 with PMF technique were firstly performed with possible factor number of 2-8. It was  
89 found that four factors solution splits clearly OA factors, with solutions of 3 or 5 factors  
90 show less or over split features. Results for factor number determination were shown in  
91 Fig.S2-5. For example, three factors solution does not split two major primary OA  
92 factors of cooking-like OA (COA) and hydrocarbon-like OA (HOA) in urban area, and  
93 five factor solutions over split the oxygenated organic aerosol, thus four factors solution  
94 was finally determined as the best. However, previous studies demonstrate that PMF  
95 solution sometimes failed in clean separating OA factors<sup>1,2</sup>. Similar case was also  
96 found in the unconstrained solution as shown in Fig.S4 that the factor 1 showed obvious  
97 cooking-like primary OA (COA) features (for example high correlations with m/z 55,  
98 and obvious noon peak), however showing higher oxidation feature than previously  
99 reported results of COA with exceptionally high m/z 44 fraction<sup>2</sup>, thus the solution has  
100 defects. The a-value approach of ME-2 techniques provides additional constrains on  
101 factors through introducing user defined external factor mass spectra profile, however  
102 a priori mass spectra of COA for Q-ACSM measurements in Guangzhou urban area is  
103 lacking. Chinese spring festival (area shaded with pink color in Figure 1 of the  
104 manuscript) was during the observation period and stay home policy was recommended  
105 by Chinese government due to the COVID-19 epidemic, thus very small traffic flow  
106 however might even higher cooking activities than usual due to the festival celebration.  
107 Results of Guo, et al. (2020)<sup>2</sup> demonstrate that COA usual contribute even slightly  
108 higher than HOA (Hydrocarbon-like OA), suggesting that the dominant contribution of  
109 COA to primary OA during the special “spring festival and COVID epidemic stay home”  
110 period, thus provide us a unique opportunity to identify spectra profile that most close  
111 to realistic COA spectra. The unconstrained PMF technique performed specific to the  
112 spring festival period from 11<sup>th</sup> to 25<sup>th</sup> February 2021, and five factor solution with most  
113 prominent COA features was determined (Fig.S6-7) although might over spilt the  
114 oxygenated OA. The factor with obvious COA feature was chosen as the used defined  
115 external spectra in ME-2 of four factor solutions with a values range from 0.1 to 0.5.

116 The ME-2 solution with a value of 0.2 was adopted based on correlation coefficients  
117 with external tracers, and solutions of a values ranging from 0.1 to 0.3 as well as their  
118 correlation coefficients with external tracers are shown in Fig.S8-10. Compared with  
119 results of the unconstrained PMF, correlations of COA factor with m/z 55 has improved  
120 substantially ( $R^2$  increased from 0.49 to 0.77), and the determined COA factor has much  
121 better COA features and lower O/C <sup>3</sup>. Note the O/C value of factors were estimated  
122 using the empirical relationship between  $f_{44}$  and O/C proposed by Aiken, et al. (2008)<sup>4</sup>.  
123  
124  
125

127 **Figure S2.** Diagnostic plots of the 4-factor solution in the unconstrained PMF.

128

129

130

131

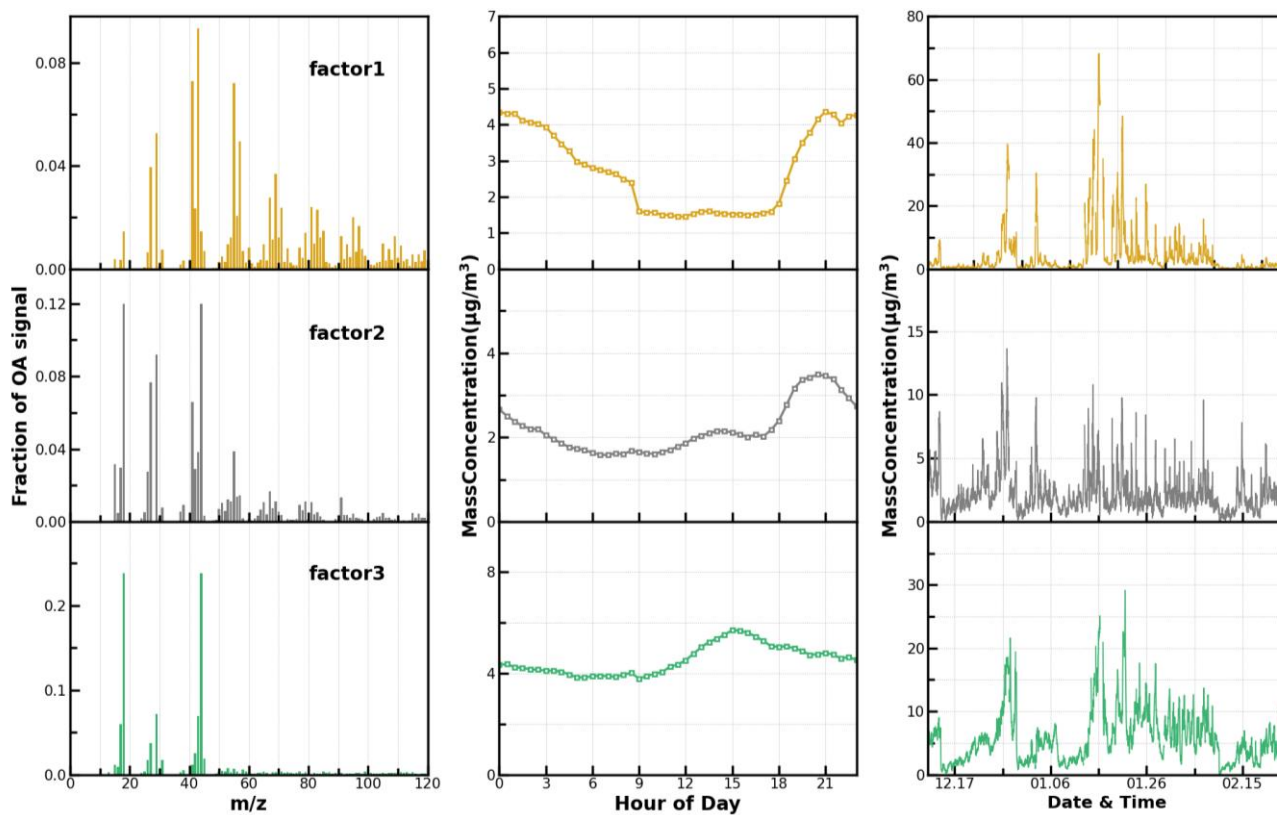
132

133

134

135

136 PMF results



137 **Figure S3.** Mass spectra, diurnal variations and time series of 3-factor solution from  
138 unconstrained PMF.

139

140

141

142

143

144

145

146

147

148

149

150

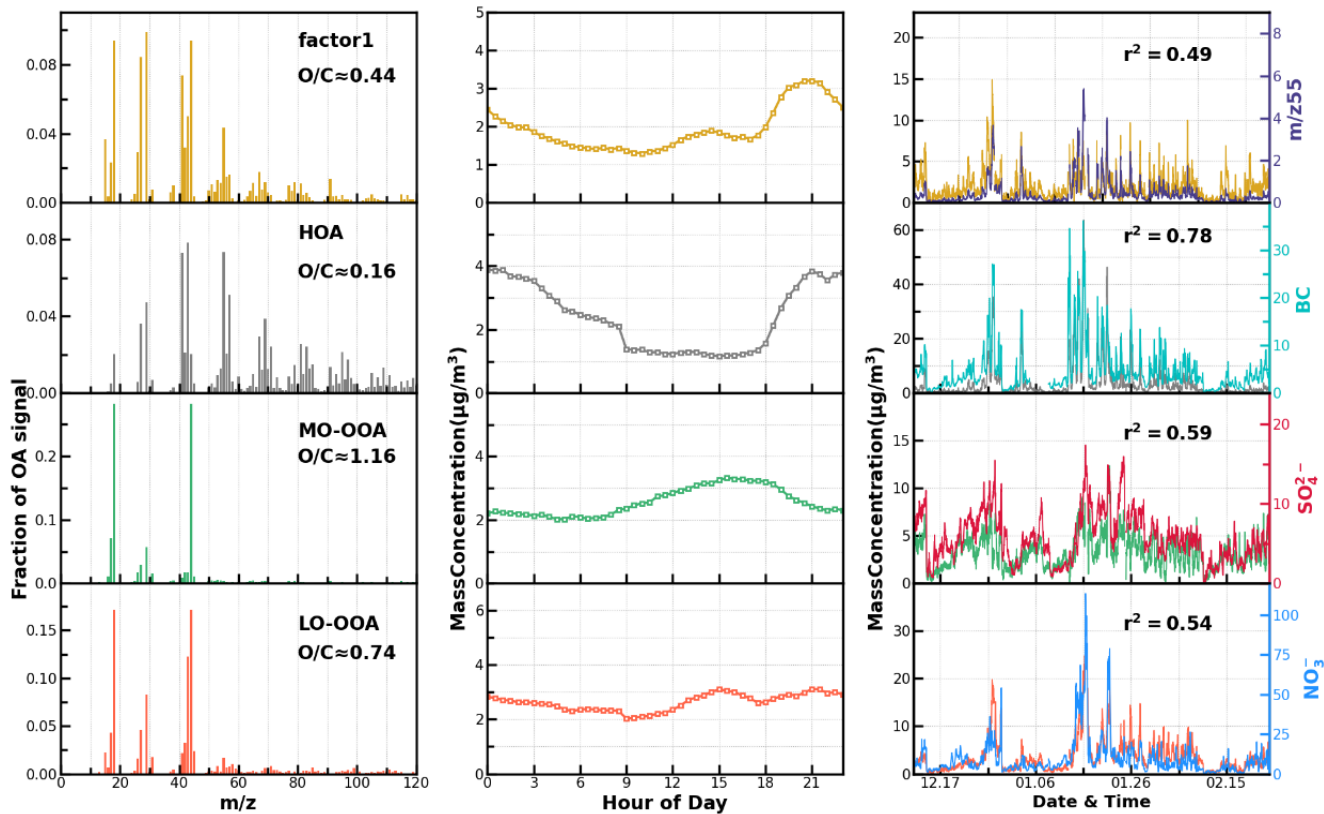
151

152

153

154

155

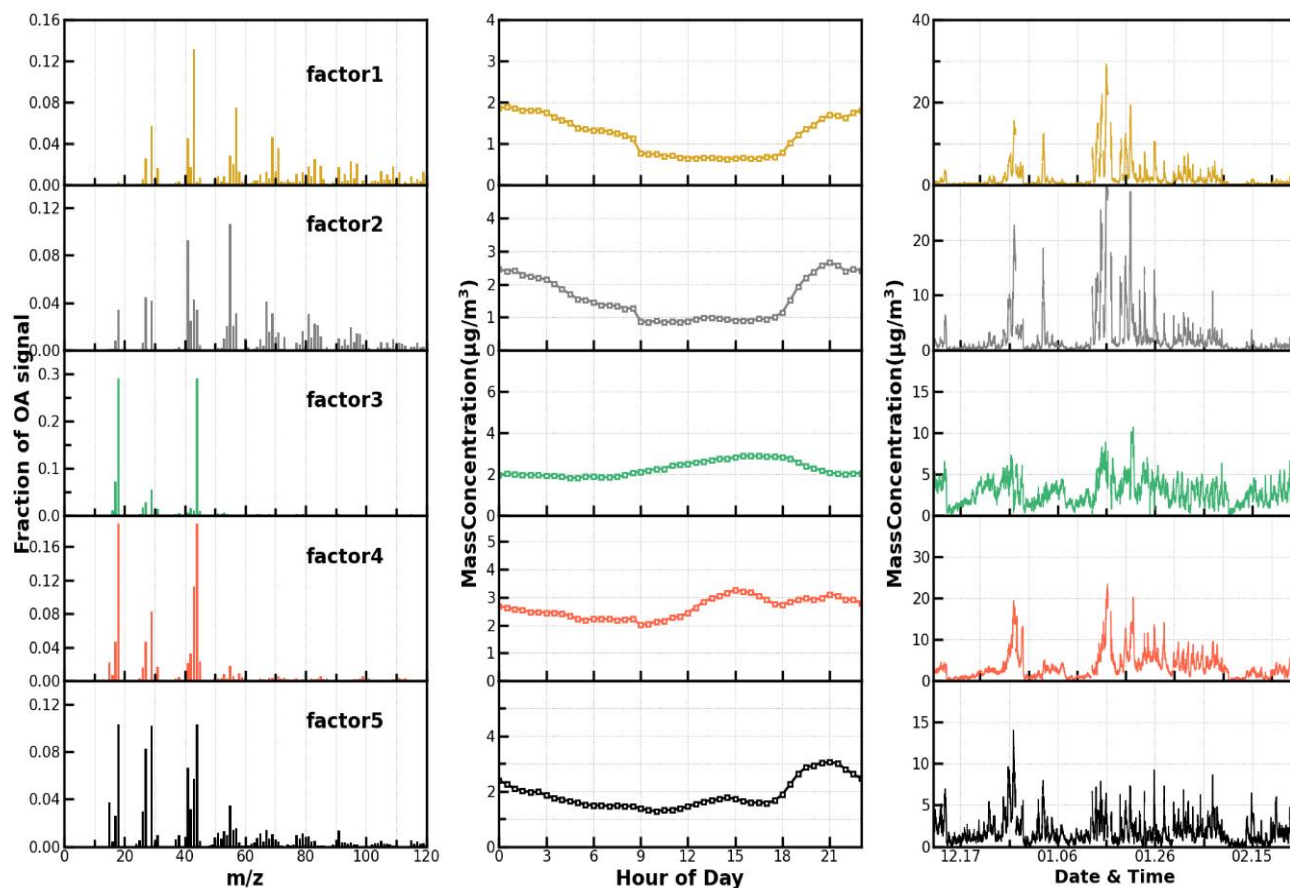


156 **Figure S4.** Mass spectra, diurnal variations, and time series of 4-factor solution from  
 157 unconstrained PMF.

158  
 159  
 160  
 161  
 162  
 163  
 164  
 165  
 166  
 167  
 168  
 169  
 170  
 171  
 172  
 173  
 174  
 175



176



177 **Figure S5.** Mass spectra, diurnal variations, and time series of 5-factor solution from  
178 unconstrained PMF.

179

180

181

182

183

184

185

186

187

188

189

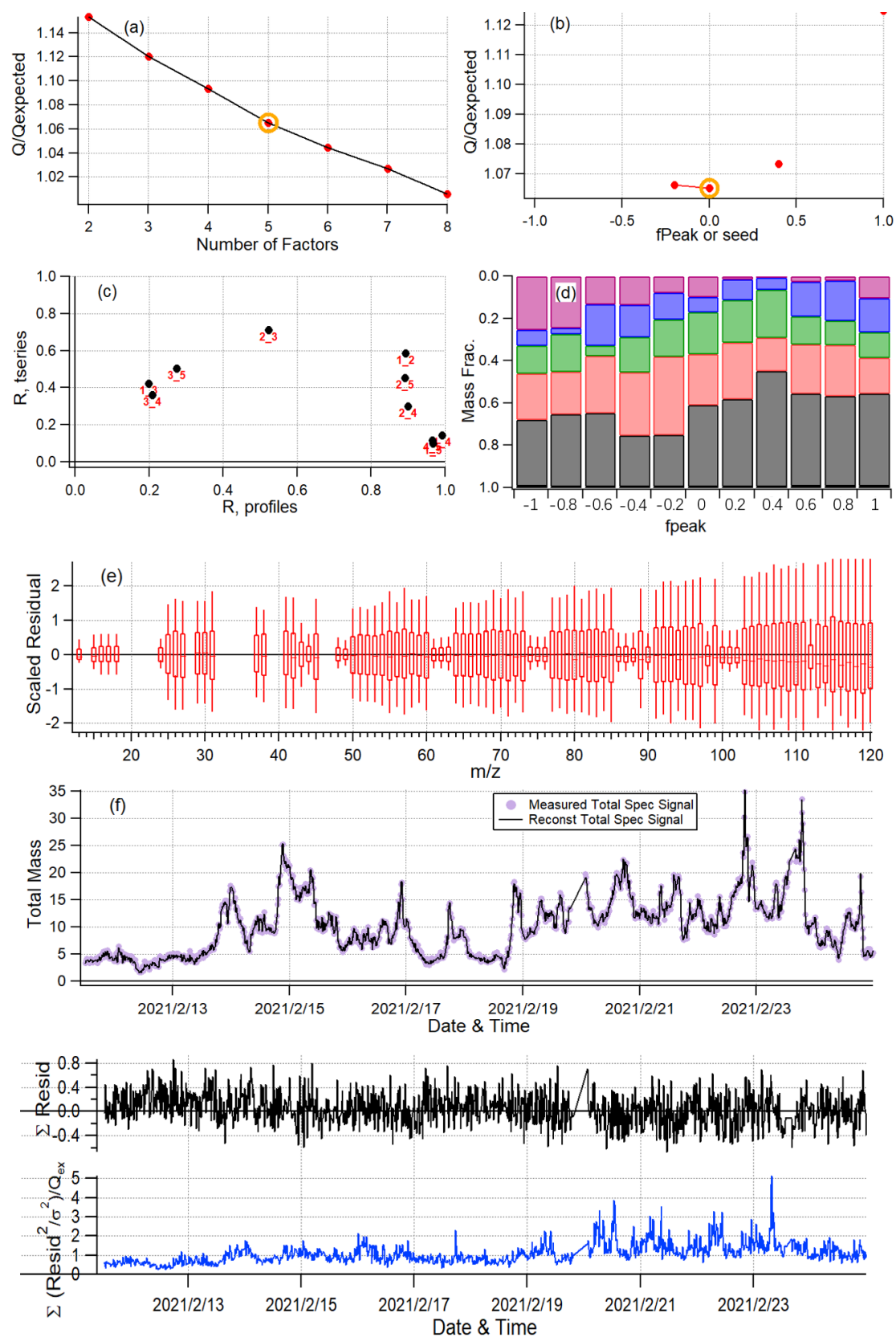
190

191

192

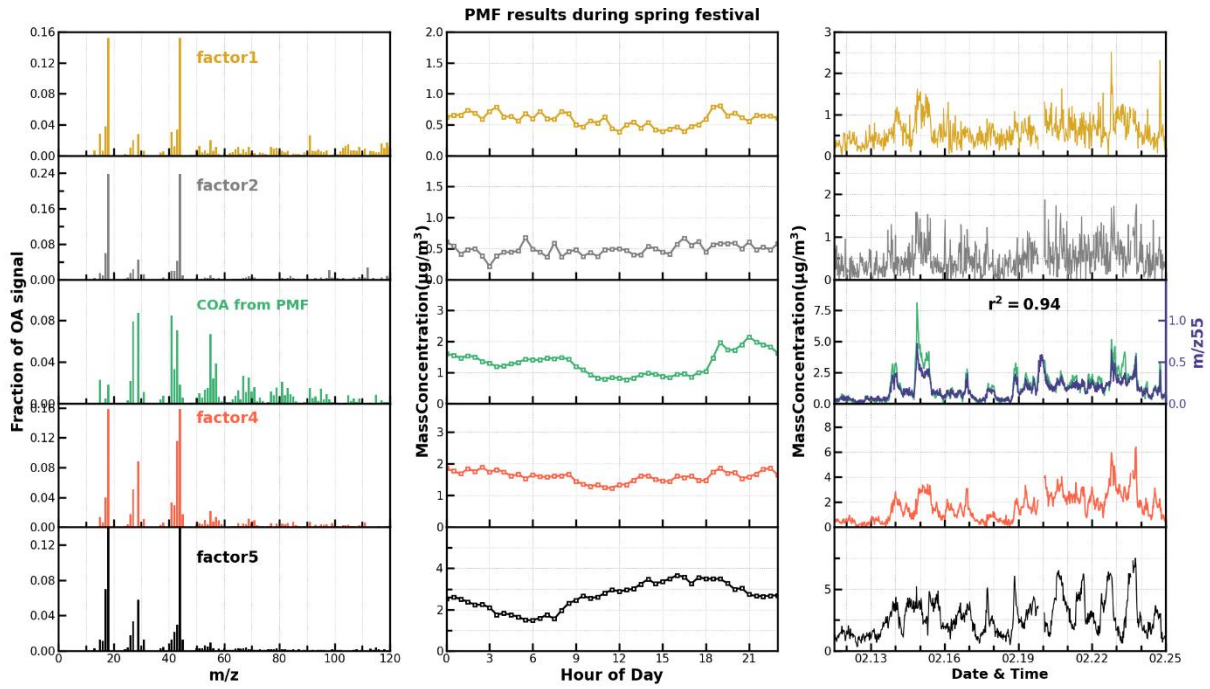
193

194



195 **Figure S6.** Diagnostic plots of the 5-factor solution in the unconstrained PMF during  
 196 the spring festival period from 11th to 25th February 2021.

197  
198  
199  
200  
201  
202



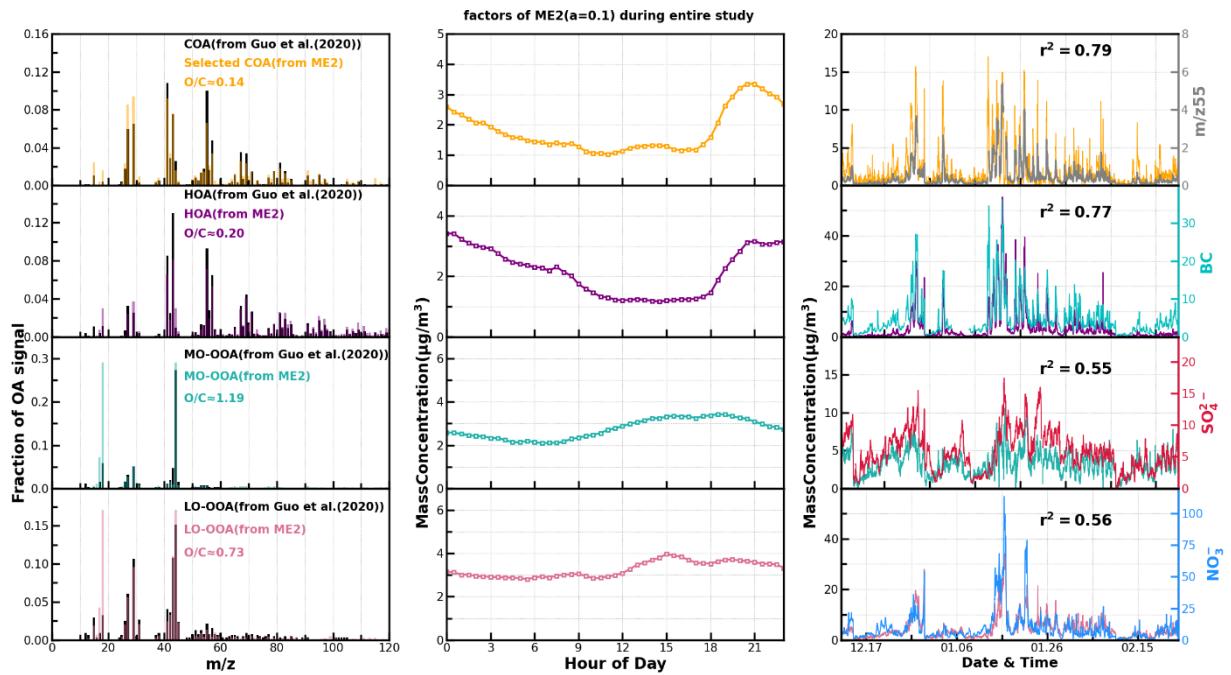
203 **Figure S7.** Mass spectra, diurnal variations, and time series of 5-factor solution from  
204 unconstrained PMF during the spring festival period from 11<sup>th</sup> to 25<sup>th</sup> February 2021.

205  
206  
207  
208  
209  
210  
211  
212  
213  
214  
215  
216  
217  
218  
219  
220  
221  
222

223  
224  
225

226 **ME-2 results**

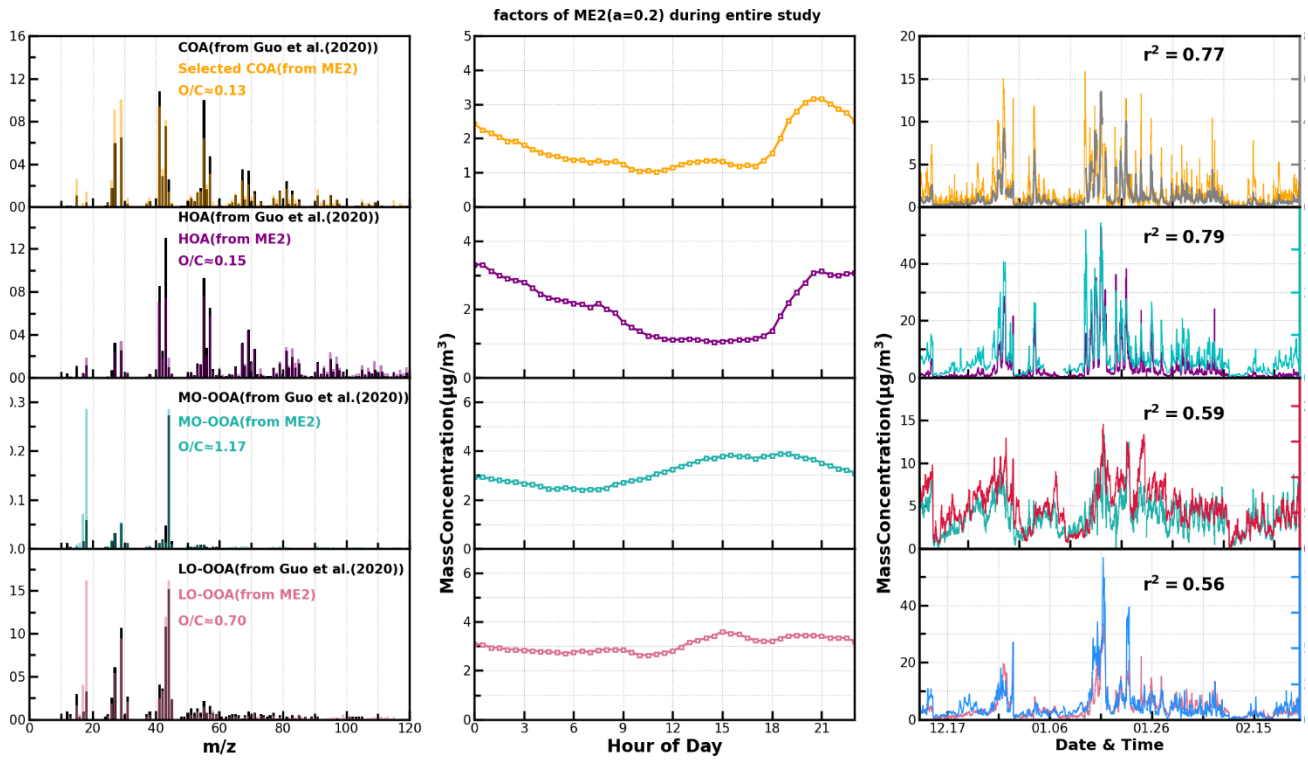
227



228 **Figure S8.** Mass spectra, diurnal variations, and time series of ME-2(a-value=0.1)  
229 under the 4-factor solution.

230  
231  
232  
233  
234  
235  
236  
237  
238  
239  
240  
241  
242  
243  
244  
245  
246

247  
248  
249

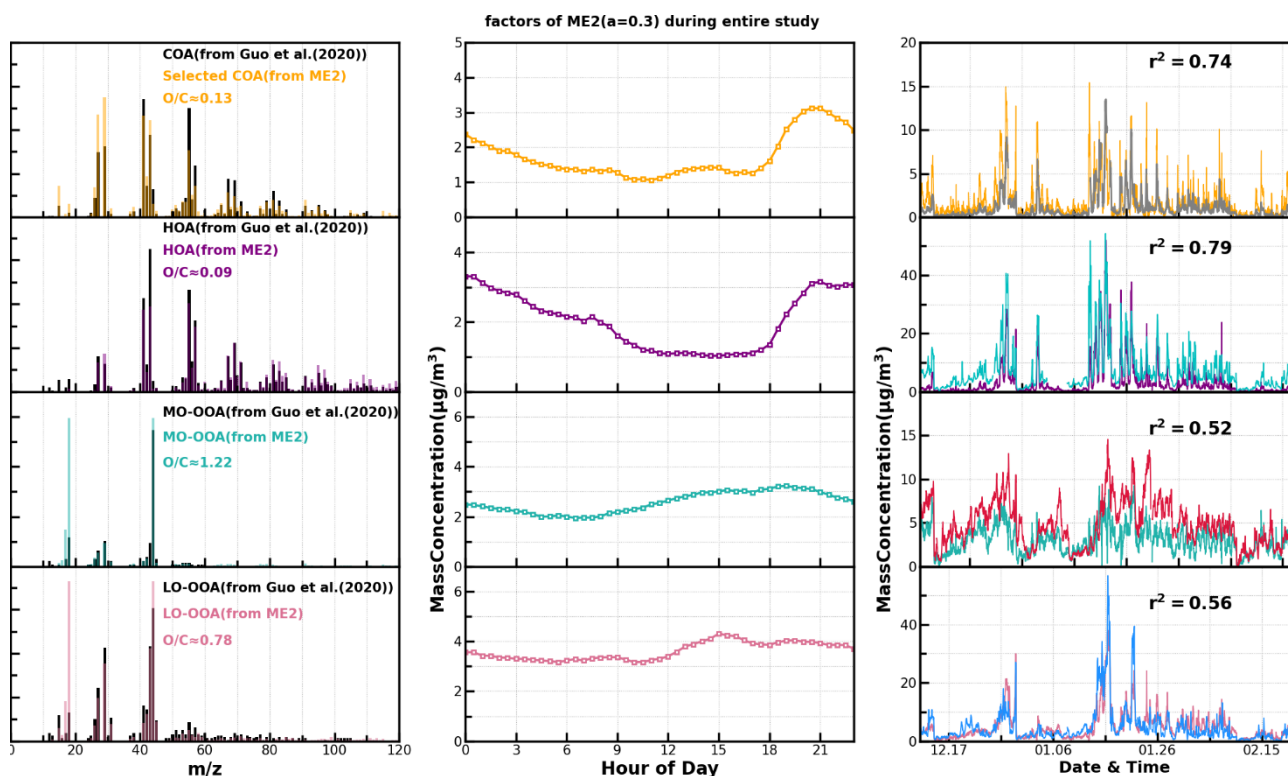


250 **Figure S9.** Mass spectra, diurnal variations, and time series of ME-2(a-value=0.2)  
251 under the 4-factor solution.

252  
253  
254  
255  
256  
257  
258  
259  
260  
261  
262  
263  
264  
265  
266  
267  
268  
269  
270

271

272



273 **Figure S10.** Mass spectra, diurnal variations, and time series of ME-2(a-value=0.3)  
 274 under the 4-factor solution.

275

276

### 277 3. Discussions on traditional multilinear regression model

278 In this study, we tried to perform the traditional multiple linear regression analysis  
 279 with HOA, COA, LOOA, MOOA, AS (ammonium sulfate), AN (ammonium nitrate)  
 280 and BC as input variables and aerosol scattering coefficients as target variable. Note  
 281 that ammonium nitrate (AN) and ammonium sulfate (AS) were determined as the  
 282 dominant form of ammonium, and paired spot of ammonium bisulfate was treated as  
 283 AS in the multiple linear regression model due to their similarity in scattering abilities.  
 284 Negative  $MSE_{LOOA}$  were obtained if MSE values were not constrained, and MSEs of  
 285 some aerosol components deviated significantly from previously reported ranges. If  
 286 MSEs of aerosol components were constrained as positive, then an  $MSE_{LOOA}$  of zero

287 would be obtained. These results demonstrate that the multiple regression model failed  
 288 in retrieving aerosol MSE, and two reasons might be responsible for this failure. The  
 289 first one is mathematically fundamental, the application of multiple linear regression  
 290 model perform best with independent input variables, however, the square of correlation  
 291 coefficients ( $R^2$ ) between several variables were higher than 0.5 for datasets of this  
 292 study (Table.S2). For example, the square of correlation coefficients between HOA and  
 293 LOOA, between LOOA and AN, and between HOA and BC are 0.6, 0.54 and 0.78  
 294 respectively. The second reason is associated with the observations that aerosol  
 295 scattering of entire aerosol populations of  $PM_{2.5}$  were measured however part of the  
 296 aerosol mass such as  $PM_1$  dust were not identified by the mass spectrometer <sup>5,6</sup> and the  
 297 contribution of unidentified part might varies substantially <sup>7</sup>. In addition, aerosol  
 298 scattering coefficients of  $PM_{2.5}$  were measured whereas mass concentrations of  $PM_1$   
 299 were quantified.

300  
 301  
 302  
 303

304 **Table S1.** Square of correlation coefficients between aerosol components

	<b>COA</b>	<b>LOOA</b>	<b>MOOA</b>	<b>BC</b>	<b>AS</b>	<b>AN</b>
<b>HOA</b>	<b>0.37</b>	<b>0.6</b>	<b>0.11</b>	<b>0.79</b>	<b>0.16</b>	<b>0.39</b>
<b>COA</b>		<b>0.42</b>	<b>0.1</b>	<b>0.43</b>	<b>0.15</b>	<b>0.17</b>
<b>LOOA</b>			<b>0.37</b>	<b>0.57</b>	<b>0.43</b>	<b>0.54</b>
<b>MOOA</b>				<b>0.12</b>	<b>0.59</b>	<b>0.49</b>
<b>BC</b>					<b>0.22</b>	<b>0.33</b>
<b>AS</b>						<b>0.28</b>

305  
 306  
 307  
 308  
 309  
 310  
 311  
 312  
 313

314 **Table S2.** Square of correlation coefficients between changes of aerosol components for identified  
 315 cases

	$\Delta\text{COA}$	$\Delta\text{LOOA}$	$\Delta\text{MOOA}$	$\Delta\text{BC}$	$\Delta\text{AS}$	$\Delta\text{AN}$
$\Delta\text{HOA}$	<b>0.34</b>	<b>0.44</b>	<b>0.43</b>	<b>0.88</b>	<b>0.01</b>	<b>0.02</b>
$\Delta\text{COA}$		<b>0.34</b>	<b>0.56</b>	<b>0.29</b>	<b>0.05</b>	<b>0.07</b>
$\Delta\text{LOOA}$			<b>0.38</b>	<b>0.5</b>	<b>0.00</b>	<b>0.03</b>
$\Delta\text{MOOA}$				<b>0.4</b>	<b>0.12</b>	<b>0.07</b>
$\Delta\text{BC}$					<b>0.02</b>	<b>0.01</b>
$\Delta\text{AS}$						<b>0.39</b>

316  
 317  
 318  
 319  
 320  
 321  
 322  
 323  
 324  
 325  
 326  
 327  
 328  
 329  
 330  
 331  
 332  
 333  
 334

335 **4. Visibility contributions estimation**

336 Based on the Koschmieder theory, atmospheric visibility is determined by  
 337 atmospheric extinction coefficient  $\sigma_{\text{ex}}$ <sup>8</sup>:



338 
$$\text{Visibility} = \frac{K}{\sigma_{ex}} . \quad \text{Eq. S1}$$

339 Where K is the Koschmieder constant, and a value of 3.0 is usually used for Asian  
 340 people and thus also visibility meter<sup>9</sup>. The  $\sigma_{ex}$  is the total atmospheric light extinction  
 341 coefficient at 550 nm caused by aerosols and air molecules and can be calculated  
 342 through the sum of its scattering and absorption components:

343 
$$\sigma_{ex} = \sigma_{sp} + \sigma_{abs} + \sigma_{air} + \sigma_{NO_2}, \quad \text{Eq. S2}$$

344 where  $\sigma_{sp}$  and  $\sigma_{abs}$  are the aerosol scattering and absorption coefficients,  $\sigma_{air}$  is  
 345 the Rayleigh scattering by air molecules and  $\sigma_{NO_2}$  the absorption by NO<sub>2</sub> molecules.  
 346 Rayleigh scattering of air molecules at 550 nm under standard atmospheric pressure is  
 347 about 13 Mm<sup>-1</sup><sup>10</sup>. The NO<sub>2</sub> absorption at 550 nm is calculated using  $\sigma_{NO_2} = 0.33 \cdot$   
 348  $[NO_2]$ , where  $[NO_2]$  represents the NO<sub>2</sub> volume mixing ratio in units of ppb, and unit of  
 349 calculated  $\sigma_{NO_2}$  is Mm<sup>-1</sup>. Aerosol absorptions at 520 and 590 nm measured by the  
 350 AE33 aethalometer were used to calculate aerosol absorptions ( $\sigma_{abs}$ ) at 550 nm through  
 351 absorption Ångström law.

352 As to the aerosol scattering  $\sigma_{sp}$  at 550 nm, it can be calculated as based on  
 353 analysis of Xu, et al. (2020)<sup>9</sup>:

354 
$$\sigma_p = \sigma_{sp,fine} + \sigma_{sp,coarse} = \sigma_{sp,PM_{2.5}}(RH) + 0.036 \cdot \sigma_{sp,PM_{2.5}}(dry) \quad \text{Eq. S3}$$

355 Where direct measurements of  $\sigma_{sp,PM_{2.5}}(dry)$  at 525 nm were converted to  
 356  $\sigma_{sp,PM_{2.5}}(dry)$  at 550 nm using measured between scattering Ångström exponent by the  
 357 nephelometer. The  $\sigma_{sp,PM_{2.5}}(RH)$  values at 525 nm were firstly calculated as the  
 358 summation of aerosol scattering coefficients of MOOA, LOOA, HOA, COA, BC, AN  
 359 and AS under ambient RH conditions by considering MSE values derived at 525 nm  
 360 and aerosol hygroscopicity:

361 
$$\sigma_{sp,PM_{2.5}}(RH) = \sigma_{sp,MOOA,PM_{2.5}}(RH) + \sigma_{sp,LOOA,PM_{2.5}}(RH) + \sigma_{sp,HOA,PM_{2.5}}(RH) +$$
  
 362 
$$\sigma_{sp,COA,PM_{2.5}}(RH) + \sigma_{sp,BC,PM_{2.5}}(RH) + \sigma_{sp,AS,PM_{2.5}}(RH) + \sigma_{sp,AN,PM_{2.5}}(RH) \quad \text{Eq. S4}$$

363 COA, BC, HOA are hydrophobic with hygroscopic parameter  $\kappa$  of zero. Thus, their  
 364 scattering didn't change with ambient RH and are same with their values in dry state.

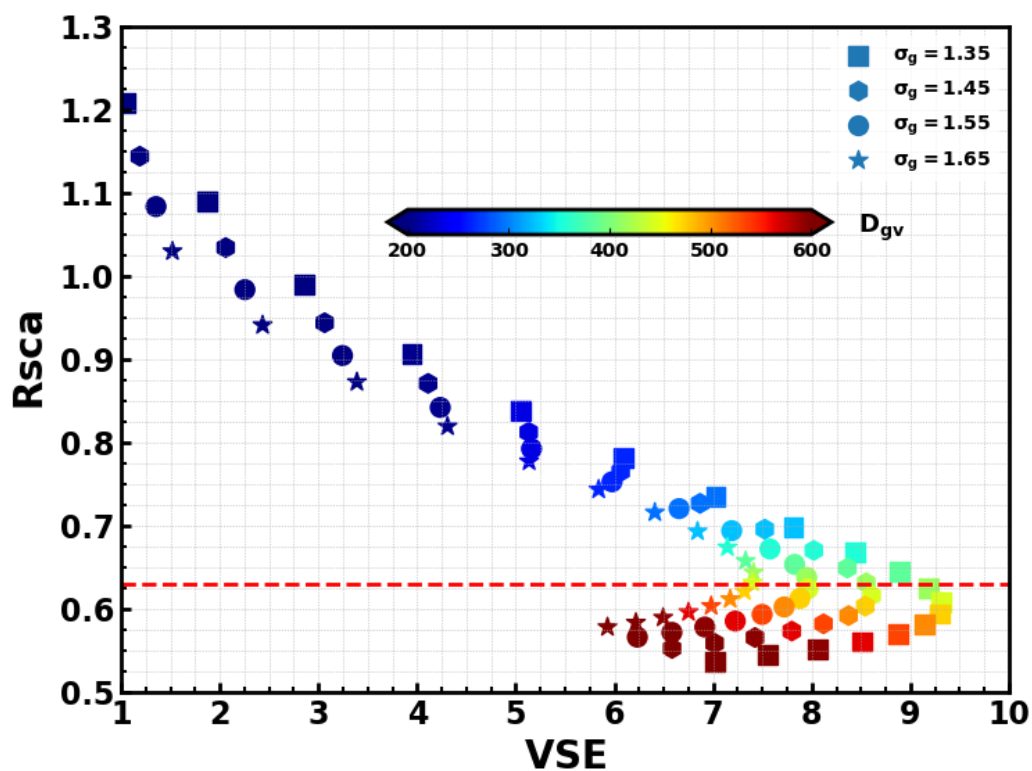
365 In addition, as discussed in Sect.4.2 of the manuscript, most HOA, COA and BC mass  
366 reside in PM1. Thus,  $\sigma_{sp,HOA,PM_{2.5}}(RH) = [HOA]_{PM1} \times MSE_{HOA,PM1}(dry)$  ,  
367  $\sigma_{sp,COA,PM_{2.5}}(RH) = [COA]_{PM1} \times MSE_{COA,PM1}(dry)$  , and  $\sigma_{sp,BC,PM_{2.5}}(RH) =$   
368  $[BC]_{PM1} \times MSE_{BC,PM1}(dry)$  where [X] represents mass concentrations of aerosol  
369 components [X]. For hydrophilic aerosol components, MOOA, LOOA, AS, and AN,  
370 their scattering under ambient RH conditions were calculated using  
371  $\sigma_{sp,MOOA,PM_{2.5}}(RH) = [MOOA]_{PM1} \times MSE_{MOOA}^* \times \kappa_{MOOA} \times R_{sca,MOOA}$  ,  
372  $\sigma_{sp,LOOA,PM_{2.5}}(RH) = [LOOA]_{PM1} \times MSE_{LOOA}^* \times \kappa_{LOOA} \times R_{sca,LOOA}$  ,  
373  $\sigma_{sp,AS,PM_{2.5}}(RH) = [AS]_{PM1} \times MSE_{AS}^* \times \kappa_{AS}(RH) \times R_{sca,AS}$ , and  $\sigma_{sp,AN,PM_{2.5}}(RH) =$   
374  $[AN]_{PM1} \times MSE_{AN}^* \times \kappa_{AN}(RH) \times R_{sca,AN}$ . As discussed in Sect.4.4 of the manuscript,  
375  $R_{sca,LOOA}$  is 0.87, and 0.63 for  $R_{sca,MOOA}$ ,  $R_{sca,AS}$  and  $R_{sca,AN}$ .  $MSE_X^*$  defined as  
376  $MSE_X^* = \frac{\sigma_{sp,525}(PM_{2.5})}{[X](PM_1)}$  for aerosol components were retrieved and discussed in Sect.4.2  
377 of the manuscript.  $\sigma_{sp,X,PM_{2.5}}(RH)$  values at 550 nm of aerosol components X were  
378 then converted to 550 nm using measured scattering Ångström exponent. Contributions  
379 of aerosol components to visibility degradation were thus calculated as:

$$380 \quad Contribution = \frac{\sigma_{sp,X,PM_{2.5}}(RH, 550 \text{ nm})}{\sigma_{ex}(550 \text{ nm})}$$

381  
382  
383  
384  
385  
386  
387  
388

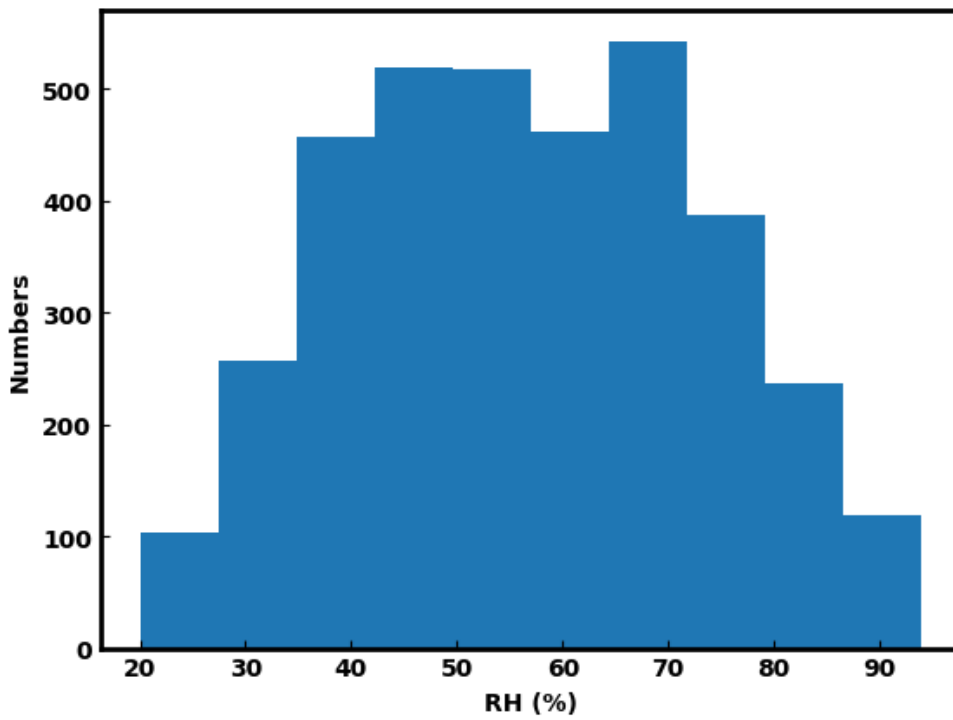
## 389 5. Other Figures

390  
391  
392



394 **Figure S11.** Simulated relationships between  $VSE_{PM1}$  and  $R_{sca}$  using Mie theory  
395 through varying volume geometric mean  $D_{gv}$  of lognormal size distributions from 100  
396 to 700 nm under different standard deviation ( $\sigma_g$ ) conditions.

397

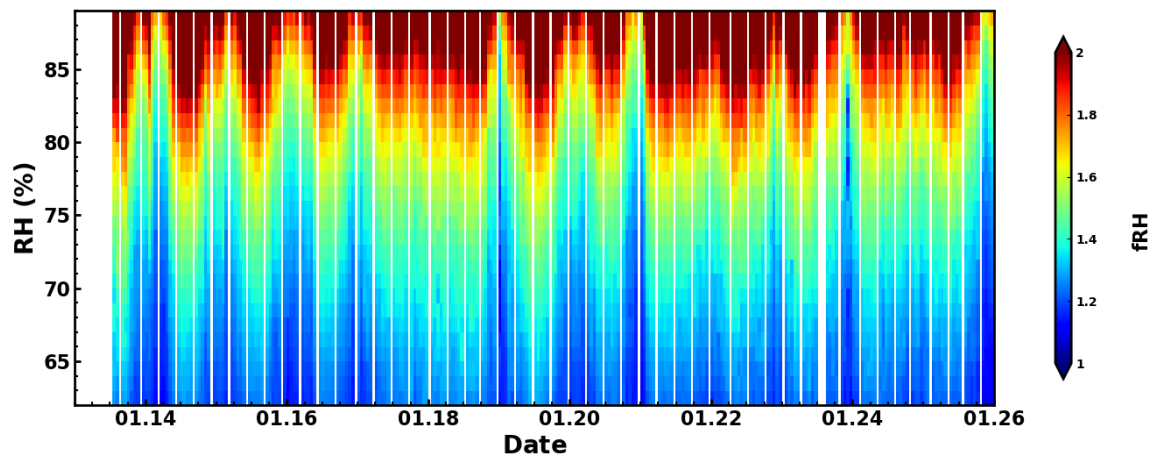


399 **Figure S12.** Histogram of ambient relative humidity (RH) during the observation  
400 period.

401  
402  
403  
404  
405  
406  
407  
408  
409  
410  
411

412

413



414 **Figure S13.** Aerosol light scattering enhancement measurements (fRH) at 525 nm from  
415 13<sup>th</sup> to 26<sup>th</sup> February with RH range of 60-90%.

416

417

418

419

420

421

422

423

424

425

426

427

428

429

430

431

432

433

434

435

436

437

438

439

440

441

442  
443  
444  
445  
446  
447  
448

449 **References**

- 450 1. Canonaco, F.; Crippa, M.; Slowik, J. G.; Baltensperger, U.; Prévôt, A. S. H., SoFi, an IGOR-based  
451 interface for the efficient use of the generalized multilinear engine (ME-2) for the source  
452 apportionment: ME-2 application to aerosol mass spectrometer data. *Atmos. Meas. Tech.* **2013**,  
453 *6*, (12), 3649-3661.
- 454 2. Guo, J.; Zhou, S.; Cai, M.; Zhao, J.; Song, W.; Zhao, W.; Hu, W.; Sun, Y.; He, Y.; Yang, C.; Xu, X.;  
455 Zhang, Z.; Cheng, P.; Fan, Q.; Hang, J.; Fan, S.; Wang, X.; Wang, X., Characterization of submicron  
456 particles by time-of-flight aerosol chemical speciation monitor (ToF-ACSM) during wintertime:  
457 aerosol composition, sources, and chemical processes in Guangzhou, China. *Atmospheric*  
458 *Chemistry and Physics* **2020**, *20*, (12), 7595-7615.
- 459 3. Sun, Y. L.; Wang, Z. F.; Fu, P. Q.; Yang, T.; Jiang, Q.; Dong, H. B.; Li, J.; Jia, J. J., Aerosol  
460 composition, sources and processes during wintertime in Beijing, China. *Atmos. Chem. Phys.* **2013**,  
461 *13*, (9), 4577-4592.
- 462 4. Aiken, A. C.; DeCarlo, P. F.; Kroll, J. H.; Worsnop, D. R.; Huffman, J. A.; Docherty, K. S.; Ulbrich,  
463 I. M.; Mohr, C.; Kimmel, J. R.; Sueper, D.; Sun, Y.; Zhang, Q.; Trimborn, A.; Northway, M.; Ziemann,  
464 P. J.; Canagaratna, M. R.; Onasch, T. B.; Alfarra, M. R.; Prevot, A. S. H.; Dommen, J.; Duplissy, J.;  
465 Metzger, A.; Baltensperger, U.; Jimenez, J. L., O/C and OM/OC Ratios of Primary, Secondary, and  
466 Ambient Organic Aerosols with High-Resolution Time-of-Flight Aerosol Mass Spectrometry.  
467 *Environmental science & technology* **2008**, *42*, (12), 4478-4485.
- 468 5. Shao, L.; Li, W.; Yang, S.; Shi, Z.; Lü, S., Mineralogical characteristics of airborne particles  
469 collected in Beijing during a severe Asian dust storm period in spring 2002. *Science in China Series*  
470 *D: Earth Sciences* **2007**, (6), 953-959.
- 471 6. Ng, N. L.; Herndon, S. C.; Trimborn, A.; Canagaratna, M. R.; Croteau, P. L.; Onasch, T. B.; Sueper,  
472 D.; Worsnop, D. R.; Zhang, Q.; Sun, Y. L.; Jayne, J. T., An Aerosol Chemical Speciation Monitor  
473 (ACSM) for Routine Monitoring of the Composition and Mass Concentrations of Ambient Aerosol.  
474 *Aerosol Science and Technology* **2011**, *45*, (7), 780-794.
- 475 7. Kuang, Y.; He, Y.; Xu, W.; Zhao, P.; Cheng, Y.; Zhao, G.; Tao, J.; Ma, N.; Su, H.; Zhang, Y.; Sun,  
476 J.; Cheng, P.; Yang, W.; Zhang, S.; Wu, C.; Sun, Y.; Zhao, C., Distinct diurnal variation in organic  
477 aerosol hygroscopicity and its relationship with oxygenated organic aerosol. *Atmos. Chem. Phys.*  
478 **2020**, *20*, (2), 865-880.
- 479 8. Chen, J.; Zhao, C. S.; Ma, N.; Liu, P. F.; Göbel, T.; Hallbauer, E.; Deng, Z. Z.; Ran, L.; Xu, W. Y.;  
480 Liang, Z.; Liu, H. J.; Yan, P.; Zhou, X. J.; Wiedensohler, A., A parameterization of low visibilities for  
481 hazy days in the North China Plain. *Atmos. Chem. Phys.* **2012**, *12*, (11), 4935-4950.
- 482 9. Xu, W.; Kuang, Y.; Bian, Y.; Liu, L.; Li, F.; Wang, Y.; Xue, B.; Luo, B.; Huang, S.; Yuan, B.; Zhao, P.;  
483 Shao, M., Current Challenges in Visibility Improvement in Southern China. *Environmental Science*

484 & *Technology Letters* **2020**.

485 10. Liu, X.; Cheng, Y.; Zhang, Y.; Jung, J.; Sugimoto, N.; Chang, S.-Y.; Kim, Y. J.; Fan, S.; Zeng, L.,  
486 Influences of relative humidity and particle chemical composition on aerosol scattering properties  
487 during the 2006 PRD campaign. *Atmospheric Environment* **2008**, *42*, (7), 1525-1536.

488